JOURNAL OF PROPULSION AND POWER
Vol. 26, No. 3, May–June 2010

Technical Notes

Blade Bowing Effect on Aerodynamic Performance of a Highly Loaded Turbine Cascade

Chunqing Tan,* Hualiang Zhang,† Hongde Xia,‡ and Haisheng Chen§
Chinese Academy of Sciences, 100190 Beijing, People's Republic of China
and
Atsumasa Yamamoto¶
Japan Aerospace Exploration Agency, Tokyo 182-8522, Japan

DOI: 10.2514/1.45308

Introduction

AS ONE of the major measures to improve the aerodynamic performance of modern turbines, highly loaded blades (blades with a high-turning angle) have attracted much attention in the past two decades [1–7]. However, it is found that due to the high-turning angle, the highly loaded blades cause high loss because of the serious secondary flow and centralized vortices [1–7]. Blade bowing (compound leaning or curving) has been recognized as an effective way to reorganize the vortices, reduce the secondary flow loss, and improve the efficiency of turbines [4–8], and also the fundamental for the three-dimensional optimization of turbine blades [6,9–11]. It is therefore the primary motivation of this work to find out whether the blade bowing applies to improving the performance of the highly loaded turbine cascade (turning angle 113 deg). The second motivation of this paper is to carry out a systematic study with a series of negatively and positively bowed highly loaded blades. (When the dihedral angle between the blade pressure side and cascade endwalls is acute, the bowed angle is positive and vice versa). Clearly there is a vacuum of such a systematic study in highly loaded turbine cascades, as only few certain bowing angles were investigated individually [4,5,8].

Experimental and Analysis Methods

Totally seven sets of cascades (−30, −20, −10, 0, 10, 20, and 30 deg) were investigated. Experimental work was conducted with a low-speed linear cascade wind tunnel. The test blade profile and spanwise blade stacking line are shown in Fig. 1. The geometric coordinates of the blade profile [2] and the experimental and analysis methods [7] can be found elsewhere. Specific geometrical and aerodynamic parameters of the cascade are shown in Tables 1 and 2.

Received 5 May 2009; revision received 15 February 2010; accepted for publication 16 February 2010.

*Head, Laboratory of Propulsion and Power, Institute of Engineering Thermophysics. Member AIAA.
†Postdoctoral Research Fellow, Institute of Engineering Thermophysics.
‡Research Officer, Institute of Engineering Thermophysics.
§Professor, Institute of Engineering Thermophysics; chen_hs@mail.etp.ac.cn. (Corresponding Author).
¶Research Officer, Aircraft Propulsion Research Center.

There were two measurement planes located at 26 mm upstream from the cascade leading edge and 17 mm downstream from the cascade trailing edge, respectively. The pitchwise measurement width was 1.29 blade pitches. A five-hole pitot microprobe with a head size of 1.5 mm was used to measure the cascade flowfields. Periodicity was checked using oil surface flow visualization, surface static tappings on the blades, and five-hole probe traverses. The measurement error of the pressure is 0.5% and the error in overall mass-averaged total loss coefficient is estimated to be ±0.002. Oil flow visualization was conducted by using a mixture of titanium dioxide, oleic acid, liquid paraffin, and dye. The white oil paints were first applied to the brown blade surfaces, and then the tunnel ran at preset conditions for ∼10 min; thus, the oil paints could produce the clear flow patterns on blade surfaces (longer duration times led to no detectable difference).

In the following analysis, oil visualization results are first used to analyze the separation and vortex structure of the cascade flowfield by using the topological methodology [2,4,7,12]. The topological structures, including separation curves, reattachment curves, and singular points, are the marks of boundary layer that can provide much information for a qualitative analysis on the flowfields of cascades [4,6,12]. Flow parameters such as pressure, velocity, and energy loss achieved from the measured data of the five-hole probe [2,7] were used for further quantitative analysis on the three-dimensional flowfields of the cascades. The local energy loss coefficient is defined as

$$\xi = \frac{(P_s/P_t)^{(k-1)/k} - (P_s/P_{t,\text{in}})^{(k-1)/k}}{1 - (P_s/P_{t,\text{in}})^{(k-1)/k}} \tag{1}$$

where P_s, P_t, ρ, ρ_{in}, and $P_{t,\text{in}}$ represent local static pressure, local total pressure, local density, cascade inlet density, and inlet total pressure, respectively, and k is specific heat ratio of air. Because the flow separations are serious in highly loaded turbine cascade, the mixing loss caused by the secondary flow downstream from the cascade passage is not negligible. The total energy loss coefficient is defined as

$$\bar{\xi} = \frac{(P_s/P_t)^{(k-1)/k} - (P_s/P_{t,\text{in}})^{(k-1)/k}}{1 - (P_s/P_{t,\text{in}})^{(k-1)/k}} + \frac{\rho v^2/2 + \rho w^2/2}{\rho_{\text{in}} U_{\text{in}}^2/2} \tag{2}$$

where U_{in} is the inlet velocity, and v and w refer to the two components of the secondary flow vector parallel to the endwall plane and along the blade height, respectively. The definitions of secondary flow and secondary flow vorticity are identical to [1–7].

Results and Discussion

Figures 2a–2c show the oil flow visualization results on the suction surfaces. There are two major topological structures in the straight cascade (Fig. 2b): 1) the separation curves of passage vortices (L1 and L2) in both corner regions, and 2) a still patch of low-velocity fluid in the middle region (SP) on which a series of still oil points spread. These still oil points are the marks of separation bubbles due to the boundary-layer transition, according to the topological theory [12], and the flow velocity in the separation bubbles is very small.

In the positively bowed cascade (Fig. 2c), the basic topological structure of flow pattern is similar to that of straight cascade, but with two major differences. One is the location and/or scale of the basic topological structures (L1, L2, and SP), and the other is an obvious inverse flow region at the midspan. In comparison with Fig. 2b, both the separation curves (L1 and L2) in Fig. 2c move toward midspan and the startup points move upstream. This indicates that, due to the positive blade bowing, passage vortices (PVs) start up earlier and the

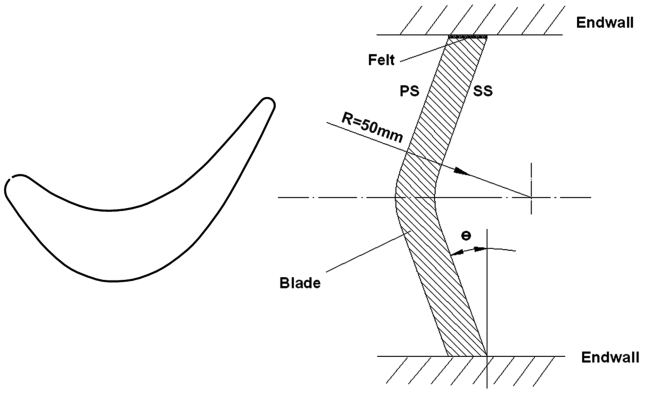

Fig. 1 Blade profile and stacking line.

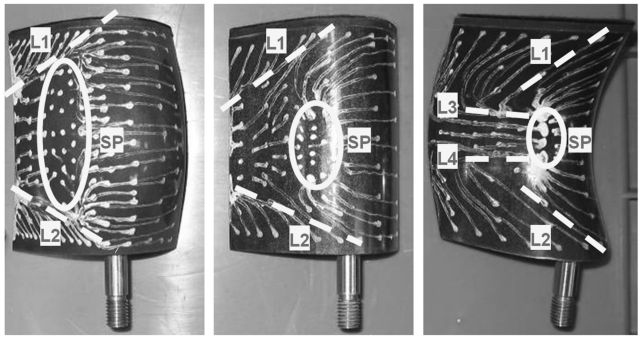

a) -20 degree **b) Straight** **c) +20 degree**

Fig. 2 Oil flow patterns on the suction surfaces.

location moves toward midspan. This could weaken the accumulation of low energy flow in the corner regions. However, the SP is smaller than that in Fig. 2b and the separation curves meet at the midspan, indicating that the passage vortices meet each other in the cascade passage. This, together with the boundary thickening at midspan due to the higher load [4,9], could cause the flow separation at the trailing edge, which is reflected by the inverse flow oil curves at the midspan of the blade surface (L3 and L4). Both the mixing and flow separation will increase the secondary flow and energy loss at midspan. The effect of negative blade bowing is opposite to the positive one. The SP area at mispan is much bigger and the downstream flow curves reattach on the blade surface. The PVs' separation curves, L1 and L2, are clearer in comparison with those of the straight cascade, and they move toward the corner regions. This could increase the mixing and energy loss in the corner regions.

Figure 3 shows secondary flow vorticity contours and secondary flow vectors at the outlet measurement plane (positive vorticity denotes the direction of vortex as anticlockwise). It can be seen that trailing-edge vortices (TVs), PVs and corner vortices (CVs) have different rotation directions and distribute alternately along the blade height. TVs and PVs have relatively greater intensity and size than corner vortices. In comparison with the straight cascade, the intensity and size of TVs in the positively bowed cascade are greater, while the intensity and size of PVs are similar. At the same time, the PVs in Fig. 3c move further away from the corner regions than those in Fig. 3b. This could reduce the mixing of the PV and the CV, hence reducing the energy loss near endwalls. On the contrary, in the negatively bowed cascade, TVs are weaker and PVs move toward endwalls (Fig. 3a). These two vortices (TV and PV) could integrate with CVs gradually at endwall regions and increase the thickness of the boundary layers and the streamwise vorticity (Fig. 3a). Accordingly, there could be more serious flow mixings of PVs, CVs, and endwall boundary layers in corner regions; see more discussion below.

Figure 4 shows the contours of the local energy loss coefficient ξ at the outlet measurement plane. The loss contours of the straight blade cascade are characterized by two high-loss cores at around $1/3$ of the blade height (Fig. 4b). The high-loss cores correspond to the high-vorticity cores in Fig. 3b. With the bowed blades (Figs. 4a and 4c) the loss contours roughly follow the blade spanwise stacking line. With increasing the blade bowing angle, the loss around the blade midspan increases, whereas that at the near endwall regions decreases. Figure 5 shows the spanwise distributions of pitch-averaged local energy losses at the outlet measurement plane where $\bar{H}$ refers to the normalized blade height. It is seen that with increasing the bowing angle, the energy loss in the midspan region increases and that in the near endwall regions the energy loss eventually decreases. The mass-averaged total energy loss coefficient $\bar{\xi}$ is shown in Fig. 6. It is obvious that the negative blade bowing increases the total energy loss, whereas appropriate positively bowed blades could decrease the total energy loss. When the positively bowed angle is $+10$ deg the overall mass-averaged total energy loss decreases to 0.157, i.e., 4.2% reduction against the straight cascade, although the improvement is not very significant. Further increasing the bowing angle, however, increases the total energy loss. When the bowed angle is $+30$ deg, the decrement of overall energy loss reduces to only 1.6%.

As shown in Fig. 3, the TVs and PVs are dominant factors in determining the flowfields of the cascades. The combination of Figs. 3–6 indicates that appropriate positively bowed blades can shift PVs to midspan and prevent the mixing of PVs and endwall boundary layers so as to decrease the energy losses in endwall regions, hence improving the overall cascade performance. At the same time, positively bowed blades increase the load at midspan, hence increasing the thickness of boundary layers at midspan. This could intensify the TVs and the secondary flow loss at midspan. This partially counteracts the beneficial effects of positive blade bowing, and consequently the overall improvement of cascade performance is not significant.

Also shown in Fig. 5 is the spanwise distribution of pitch-averaged yaw angle. One can see that in the straight cascade, the biggest underturnings, located at 30 and 70% blade height, respectively, correspond to the joint of PVs and TVs. With increasing the bowing angle, the flow underturning decreases at most blade heights because of the stronger TVs and weaker PVs (Fig. 3); meanwhile, the overturnings at endwalls diminish because the PVs depart from endwalls and reduce the transverse secondary flow. The spanwise distribution of the yaw flow angle becomes more uniform over the whole blade height with increasing bowing angle. The negative

Table 1 Geometrical and aerodynamic parameters

Parameter	Value
Number of blades M	6
Blade height H, mm	100
Chord length C, mm	73.1
Axial chord length, mm	72.6
Aspect ratio H/C	1.37
Pitch-chord ratio S/C	0.84
Blade turning angle, deg	113.0
Design inlet flow angle, deg	49.5
Design outlet flow angle, deg	−63.5
Reynolds number Re[a]	3.0×10^5
Turbulence intensity T_u, %	0.5

[a]The Reynolds number Re is defined as $\Re e = \rho V L/\mu$, where ρ, V, L, and μ refer to air density, mean air velocity at outlet, axial chord, and dynamic viscosity, respectively.

Table 2 Inlet boundary-layer parameters

Parameter	Hub	Tip
Boundary-layer thickness δ_{99}, mm	24	22
Displacement thickness δ^*, mm	2.6	2.0
Momentum thickness δ^{**}, mm	2.1	1.7
Normalized boundary-layer thickness, δ_{99}/H	0.24	0.22
Shape factor δ^*/δ^{**}	1.2	1.2

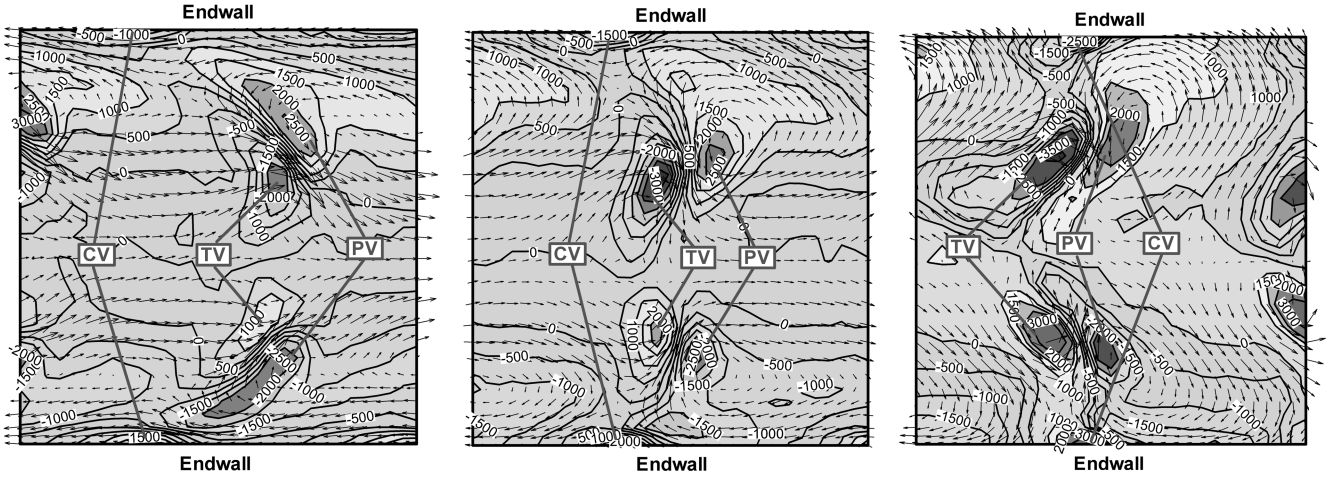

a) -20 degree b) Straight c) +20 degree

Fig. 3 Vorticity contours and secondary flow vectors at the outlet plane.

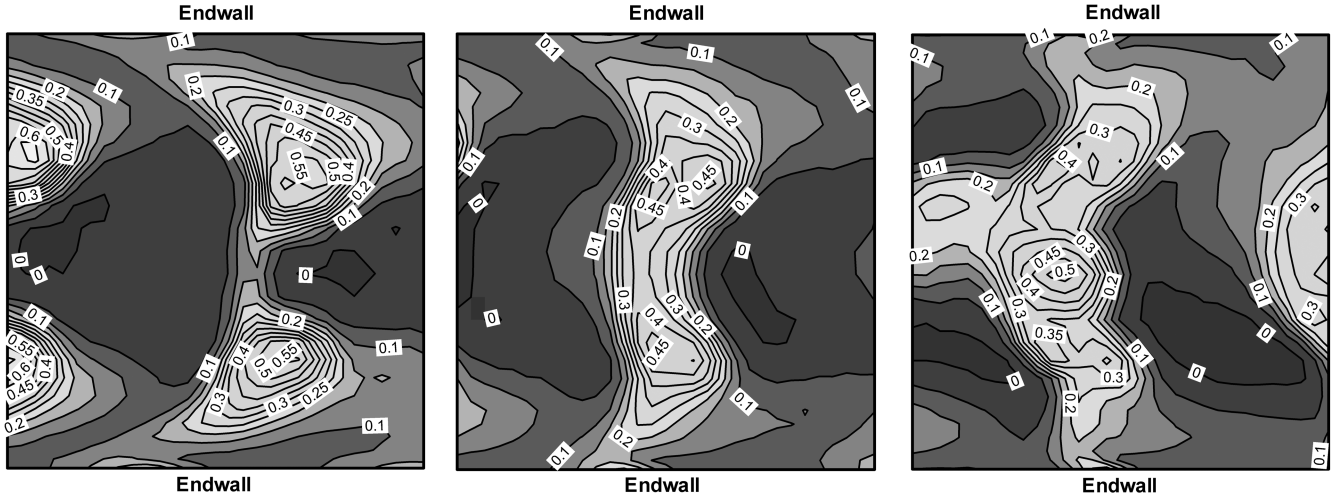

a) -20 degree b) Straight c) +20 degree

Fig. 4 Distributions of local energy loss coefficient at outlet.

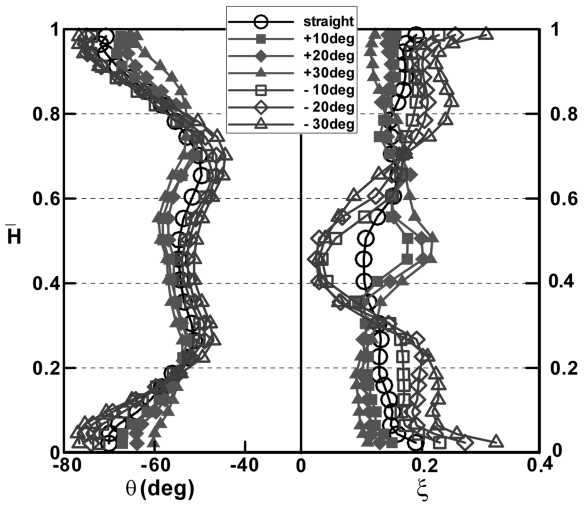

Fig. 5 Spanwise distributions of pitch-averaged local energy loss coefficient (right) and yaw angle (left).

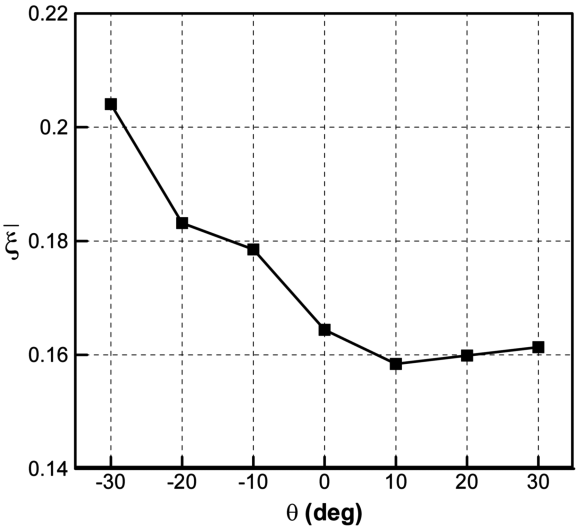

Fig. 6 Total energy loss coefficient at outlet measurement plane.

bowing deteriorates the spanwise distribution of the yaw flow angle. The overall yaw angles at the outlet are −56.72, −57.71, −57.81, −58.06, −58.00, −56.92, −56.90 for −30, −20, −10, 0, 10, 20, 30 deg cascades, respectively, which vary little and indicate little change of the overall blade load. As less uniform distribution of yaw flow angle could cause more downstream mixing energy loss [9], positive blade bowing is favorable for the test highly loaded turbine cascade in light of the yaw angle distribution.

Conclusions

The blade bowing is able to improve the aerodynamic performance of the highly loaded turbine cascade. A +10 deg bowing angle gives the optimal aerodynamic performance under conditions of this work. But the overall improvement is insignificant. The spanwise distribution of the yaw flow angle is improved by using positively bowed blades. The effects of negative blade bowing are opposite to the positive one.

Acknowledgments

The work is financially supported by 100-Talent Program of the Chinese Academy of Sciences and National Natural Science Foundation of China under grant numbers 10577019 and 50906079.

References

[1] Moustapha, S. H., Paron, G. J., and Wade, J. H. T., "Secondary Flow in Cascades of Highly Loaded Turbine Blades," *Journal of Engineering for Gas Turbines and Power*, Vol. 107, No. 4, 1985, pp. 1031–1038. doi:10.1115/1.3239807

[2] Yamamoto, A., "Production and Development of Secondary Flows and Losses in Two Types of Straight Turbine Cascades, Part II: A Rotor Case," *Journal of Turbomachinery*, Vol. 109, No. 2, 1989, pp. 194–200.

[3] Harrison, S., "Secondary Loss Generation in a Linear Cascade of High-Turning Turbine Blades," American Society of Mechanical Engineers, Paper No. 89-GT-47, 1989.

[4] Bagshaw, D. A., Ingram, G. L., Gregory-Smith, D. G., and Stokes, M. R., "An Experimental Study of Reverse Compound Lean in a Linear Turbine Cascade," *Journal of Power and Energy*, Vol. 219, No. 6, 2005, pp. 443–449. doi:10.1243/095765005X31199

[5] Han, W., Wang, Z., Tan, C., Shi, H., and Zhou, M. "Effects of Leaning and Curving of Blades with High Turning Angles on the Aerodynamic Characteristics of Turbine Rectangular Cascades," *Journal of Turbomachinery*, Vol. 116, No. 3, 1994, pp. 417–424. doi:10.1115/1.2929428

[6] Bagshaw, D. A., Ingram, G. L., Gregory-Smith, D. G., and Stokes, M. R., "An Experimental Study of Three-Dimensional Turbine Blades Combined with Profiled Endwalls," *Journal of Power and Energy*, Vol. 222, No. 1, 2008, pp. 103–110. doi:10.1243/09576509JPE478

[7] Tan, C., Yamamoto, A., Mizuki, S., and Chen, H., "Influences of Blade Bowing on Flow Fields of a Typical Stator Cascade," *AIAA Journal*, Vol. 41, No. 10, 2003, pp. 1967–1972. doi:10.2514/2.1886

[8] Harrison, S., "The Influences of Blade Lean on Turbine Losses," *Journal of Turbomachinery*, Vol. 114, No. 1, 1992, pp. 184–190. doi:10.1115/1.2927982

[9] Lampart, P., Yershov, S., and Rusanov, A., "Increasing Flow Efficiency of High-Pressure and Low-Pressure Steam Turbine Stages from Numerical Optimization of 3D Blading," *Engineering Optimization*, Vol. 37, No. 2, 2005, pp. 145–166. doi:10.1080/03052150512331315497

[10] Kfc, Y., and Zangeneh, M., "Three-Dimensional Automatic Optimization Method for Turbomachinery Blade Design," *Journal of Propulsion and Power*, Vol. 16, No. 6, 2000, pp. 1174–1181. doi:10.2514/2.5694

[11] Larocca, F., "Multiple Objective Optimization and Inverse Design of Axial Turbomachinery Blades," *Journal of Propulsion and Power*, Vol. 24, No. 5, 2008, pp. 1093–1099. doi:10.2514/1.33894

[12] Lighthill, M. J., "Attachment and Separation in Three-Dimensional Flow," *Laminar Boundary Layers*, edited by Rosenhead, Oxford Univ. Press, Oxford, England, 1963, pp. 72–82.

A. Prasad
Associate Editor